7 Event Selection

The $H \to \tau^+\tau^- \to \ell^+\ell^- 4\nu$ decay has a detector signature of exactly two light leptons (e or μ) of opposite electric charge and some amount of missing transverse energy due to the neutrinos. The lepton combinations can be either two electrons (e^+e^-), two muons ($\mu^+\mu^-$), or one electron and on muon ($e^\pm\mu^\mp$). The decay channels are labeled as ee and $\mu\mu$ for same flavour (SF) combinations and $e\mu$ or μe for different flavour (DF) combinations. The leptons and jets are each arranged according to their transverse momentum in descending order. They are labeled with integer numbers, starting with 1. The lepton or jet with the highest transverse momentum is called *leading*, the next one is denoted as *subleading*. If a quantity uses both leading and subleading lepton or jet, it will be indicated by a $\ell\ell$ or jj label, respectively.

This chapter gives an overview of the selection criteria applied to select signal candidate events. The requirements are applied to both data and simulation. Since the mass reconstruction in the $H \to \tau^+\tau^- \to \ell^+\ell^- 4\nu$ decay channel is non-trivial due to the multiple neutrinos, advanced mass reconstruction methods are introduced in Section 7.1. Triggers (Section 7.2) are used to select events with two final state leptons. After a common preselection (Section 7.3) further selection criteria are applied to select events which fall in the VBF and boosted topology (Section 7.4). This allows to separate the Higgs bosons which are produced via the VBF and ggF mechanism.

The selection introduced in this chapter will be referred to as cut-based analysis (CBA) to differentiate between the multivariate analysis (MVA) as discussed in Chapter 9, which has a slightly different event selection.

7.1 Invariant mass reconstruction

The invariant mass of the Higgs boson candidates (i.e. the invariant mass of the di-τ system) cannot be calculated without ambiguity since there are four neutrinos in the final state of the $H \to \tau_{\text{lep}}\tau_{\text{lep}}$ decay. Since the di-τ mass can be used to discriminate between signal and background processes and enables a direct measurement of the mass of the Higgs boson a, correct and precise reconstruction is needed. In the next sections two approaches are introduced, the collinear approximation and the missing mass calculator.

7.1.1 Collinear approximation

For the collinear approximation [23,24] it is assumed that the $E_{\mathrm{T}}^{\mathrm{miss}}$ originates only from the $H \to \tau\tau$ decay and that each τ-lepton is emitted in the same direction as its corresponding visible decay product (the lepton). The second assumption is called collinearity. This is a valid assumption, since $m_H/2 \gg m_\tau$, which leads to highly boosted taus.
With those two assumptions the invariant mass m_{coll} of the di-τ system can be calculated with

$$m_{\mathrm{coll}} = \frac{m_{\ell\ell}}{\sqrt{x_1 x_2}}\,, \tag{7.1}$$

where $m_{\ell\ell}$ is the mass of the dilepton system, which is constituted of the visible decay products of the τ-lepton decay. The momentum fraction which each visible decay product holds in comparison to the decaying τ-lepton is denoted as $x_{1,2}$,

$$p_{\mathrm{T}}^{\ell_i} = x_i p_{\mathrm{T}}^{\tau_i}\,, \qquad i = 1,2\,. \tag{7.2}$$

It can be calculated with

$$x_{1,2} = \frac{p_x^{\ell_1} p_y^{\ell_2} - p_y^{\ell_1} p_x^{\ell_2}}{p_x^{\ell_1} p_y^{\ell_2} \pm E_x^{\mathrm{miss}} p_y^{\ell_{2,1}} - p_y^{\ell_1} p_x^{\ell_2} \mp E_y^{\mathrm{miss}} p_x^{\ell_{2,1}}}\,. \tag{7.3}$$

The collinear approximation works well when the di-τ system is boosted and the approximations are valid. However, if the two taus are back-to-back ($\Delta\eta(\tau_1,\tau_2) = \pi$), the missing transverse energy due to the neutrinos cancels partially and the equation system which results in Eq. (7.3) cannot be solved anymore. This can be prevented by a requirement on the η difference of the visible decay products, $\Delta\eta_{\ell\ell}$, or a direct cut on the momentum fractions, which discards events with unphysical solutions ($x < 0$ or $x > 1$).

7.1.2 Missing mass calculator

If the assumption of collinearity of the decay products of the τ-leptons is not made, there is no unique solution for the invariant mass of the di-τ system. By using on-shell conditions for the τ-lepton masses and the formula to calculate the missing transverse energy (assuming that all $E_{\mathrm{T}}^{\mathrm{miss}}$ originates from the τ-lepton decays), the following set of equations can be constructed.

$$\begin{aligned}
E_x^{\mathrm{miss}} &= p^{\mathrm{miss}_1} \sin\theta_{\mathrm{miss}_1} \cos\phi_{\mathrm{miss}_1} + p^{\mathrm{miss}_2} \sin\theta_{\mathrm{miss}_2} \cos\phi_{\mathrm{miss}_2} \\
E_y^{\mathrm{miss}} &= p^{\mathrm{miss}_1} \sin\theta_{\mathrm{miss}_1} \sin\phi_{\mathrm{miss}_1} + p^{\mathrm{miss}_2} \sin\theta_{\mathrm{miss}_2} \sin\phi_{\mathrm{miss}_2} \\
m_{\tau_1}^2 &= m_{\mathrm{miss}_1}^2 + m_{\ell_1}^2 + 2\sqrt{p^{\ell_1} + m_{\ell_1}^2}\sqrt{p^{\mathrm{miss}_1} + m_{\mathrm{miss}_1}^2} \\
&\quad - 2p^{\ell_1} p^{\mathrm{miss}_1} \cos\left(\theta_{\ell_1} - \theta_{\mathrm{miss}_1}\right) \\
m_{\tau_2}^2 &= m_{\mathrm{miss}_2}^2 + m_{\ell_2}^2 + 2\sqrt{p^{\ell_2} + m_{\ell_2}^2}\sqrt{p^{\mathrm{miss}_2} + m_{\mathrm{miss}_2}^2} \\
&\quad - 2p^{\ell_2} p^{\mathrm{miss}_2} \cos\left(\theta_{\ell_2} - \theta_{\mathrm{miss}_2}\right)
\end{aligned} \tag{7.4}$$

The known variables are the components of the missing transverse energy (E_x^{miss} and E_y^{miss}) and the momenta and invariant masses of the visible decay products of the τ-leptons (ℓ_1 and ℓ_2). Unknown are the momenta, masses, and angles (ϕ and θ) of the two neutrino systems, which are composed of two neutrinos each. These quantities are labeled with miss_1 and miss_2.
Since this system of equations is underconstrained there is no single solution. However, the different solutions have different probabilities to occur due to the matrix element of the τ-decay. The missing mass calculator (MMC) algorithm [25] scans over four of the unknown variables ($m_{\text{miss}_{1,2}}$ and $\Phi_{\text{miss}_{1,2}}$), solves the system of equations and assigns each solution the corresponding probability obtained by calculating the matrix element of the τ-decay with the solution-specific kinematics. The resolution of the E_x^{miss} and E_y^{miss} variables is also included in the scan, because the MMC algorithm is affected by the resolution of $E_{\text{T}}^{\text{miss}}$. The algorithm can fail to converge if the $E_{\text{T}}^{\text{miss}}$ is badly reconstructed. To obtain only one solution either the most probable solution can be chosen or an average over all solutions, weighted by the corresponding probability, can be calculated. In this analysis the former approach is chosen.

7.2 Trigger

Triggers are used to select events with two leptons (ee, $e\mu$[1], $\mu\mu$) in the final state. A general overview of the ATLAS trigger system was given in Section 4.2.5. Both single-lepton and dilepton triggers are used. They differ between the 2015 and 2016 data taking period due to the increase in luminosity.

Table 7.1: Single-lepton triggers and offline p_{T} thresholds for the 2015 and 2016 data set used in the $H \to \tau_{\text{lep}}\tau_{\text{lep}}$ analysis.

Lepton flavour	Year	Trigger	Threshold

Electron	2015	`HLT_e24_lhmedium_L1EM20VH`
		`HLT_e60_lhmedium`
		`HLT_e120_lhloose`
			$p_{\text{T}} > 25\,\text{GeV}$

	2016	`HLT_e26_lhtight_nod0_ivarloose`
		`HLT_e60_lhmedium_nod0`
		`HLT_e140_lhloose_nod0`
			$p_{\text{T}} > 27\,\text{GeV}$

Muon	2015	`HLT_mu20_iloose_L1MU15` `HLT_mu50`	$p_{\text{T}} > 21\,\text{GeV}$
	2016	`HLT_mu26_ivarmedium` `HLT_mu50`	$p_{\text{T}} > 28\,\text{GeV}$

[1] In this section $e\mu$ indicates all events with one electron and one muon, the differentiation between $e\mu$ and μe is not made here.

Table 7.2: Dilepton triggers offline p_{T} thresholds for the 2015 and 2016 data set used in the $H \to \tau_{\mathrm{lep}}\tau_{\mathrm{lep}}$ analysis.

Channel	Year	Trigger	Threshold
ee	2015	`HLT_2e12_lhloose_L12EM10VH`	$p_{\mathrm{T}}^{e_1,e_2} > 15\,\mathrm{GeV}$
	2016	`HLT_2e17_lhvloose_nod0`	$p_{\mathrm{T}}^{e_1,e_2} > 18\,\mathrm{GeV}$
$e\mu$	2015	`HLT_e17_loose_mu14`	$p_{\mathrm{T}}^{e} > 18\,\mathrm{GeV}, p_{\mathrm{T}}^{\mu} > 15\,\mathrm{GeV}$
	2016	`HLT_e17_lhloose_nod0_mu14`	$p_{\mathrm{T}}^{e} > 18\,\mathrm{GeV}, p_{\mathrm{T}}^{\mu} > 15\,\mathrm{GeV}$
$\mu\mu$	2015	`HLT_mu18_mu8noL1`	$p_{\mathrm{T}}^{\mu_1} > 19\,\mathrm{GeV}, p_{\mathrm{T}}^{\mu_2} > 10\,\mathrm{GeV}$
	2016	`HLT_mu22_mu8noL1`	$p_{\mathrm{T}}^{\mu_1} > 24\,\mathrm{GeV}, p_{\mathrm{T}}^{\mu_2} > 9\,\mathrm{GeV}$

The triggers for the $H \to \tau_{\mathrm{lep}}\tau_{\mathrm{lep}}$ analysis are listed in Tables 7.1 and 7.2. Multiple triggers for the same object and data taking period are combined with a logical 'or'. The overlap of single-lepton and dilepton triggers is avoided to prevent difficulties with the trigger efficiencies by selecting the triggers based on the transverse momentum of the lepton. Lower p_{T} thresholds are used for dilepton triggers and higher ones for single-lepton triggers as illustrated in Fig. 7.1.

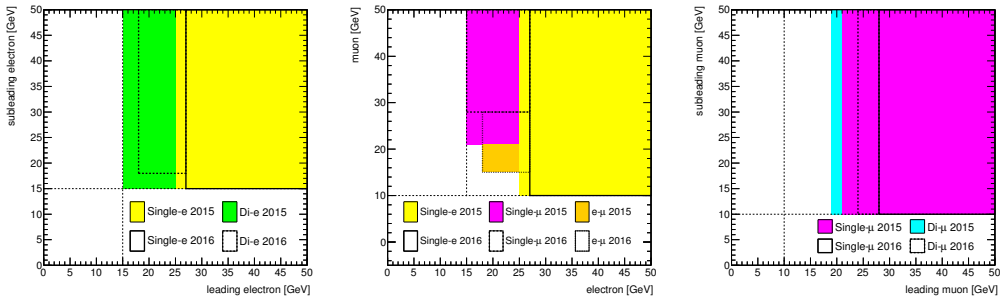

Figure 7.1: Transverse momentum criteria to select either single-lepton or dilepton triggers in order to avoid overlap. The plots correspond to ee (left), $e\mu$ (middle), and $\mu\mu$ (right) final states. [26]

Trigger names are composed of a series of acronyms and abbreviations chained together, directly or with underscores, which define the trigger type and the imposed requirements on the objects to trigger. For this analysis all trigger names start with `HLT`, indicating that the software-based High Level Trigger is used. Electrons and muons are denoted as `e` and `mu`, respectively, followed by a number defining the transverse momentum threshold in GeV, which the object has to fulfill. A preceding number corresponds to multiple objects with the same requirements. Identification and isolation criteria as introduced in Sections 6.2 and 6.3 can be imposed on the triggered objects, which is decoded as `lhID` and `iISO`, where `ID` and `ISO` specify the corresponding working points. If there is no requirement on the distance of the observed tracks to the primary vertex the term `nod0` is included. HLTs can be seeded by L1 triggers, which is indicated by including `L1` in

the trigger name. L1 trigger names also contain the type of the object to trigger, `E` and `M` for electrons and muons, respectively. Usually, there is a threshold on the missing transverse energy, denoted as `M` followed by a number, which corresponds to the threshold in GeV. The $E_{\mathrm{T}}^{\mathrm{miss}}$ thresholds can vary slightly as a function of η, which is denoted with `V`. An additional hadronic veto can be applied, which is indicated by `H`.
To account for differences in the trigger efficiencies correction factors are calculated by comparing the efficiencies between data and simulation [27, 28]. An additional offline p_{T} requirement is introduced to ensure that the trigger efficiencies are in the plateau region. The thresholds are $1-3\,\mathrm{GeV}$ higher than the trigger p_{T} thresholds. They can be found in Tables 7.1 and 7.2.

7.3 Preselection

Before requiring kinematic cuts to purify signal events a series of requirements to ensure data quality are applied.

(1) Good Run List
Data events are discarded if they are not included in the good run list, which contains the events which were recorded when all sub-detector systems have been in full operational mode. This results in an integrated luminosity of $\int \mathcal{L}\,\mathrm{d}t = 36.1\,\mathrm{fb}^{-1}$.

(2) Primary vertex
At least on reconstructed vertex is required, which is consistent with the IP. This is used to reject events from cosmic rays and beam-halo effects.

Additional requirements on the vertex?

(3) Jet cleaning and crazy muon veto
Events with jet contributions which can not be associated with hard scattering are removed [29, 30].

Crazy muon veto?

Now basic trigger and preselection cuts are applied to select the decay topology of the $H \to \tau_{\mathrm{lep}}\tau_{\mathrm{lep}}$ decay. Whenever viable, a distribution of the signal and different backgrounds is shown for a variable before the cut on this variable was applied. Normalization factors as defined in Section 8.2 are applied. Their values are 1.06 (top), 1.19 ($Z \to \ell\ell$), and 1.07 ($Z \to \tau\tau$) respectively. The signal is scaled by factor 20. The error bands only contain statistical uncertainties.

Change signal scaling to x50

(4) Number of leptons
Exactly two leptons, either two electrons, one electron and on muon, or two muons, with the reconstruction and identification criteria defined in Sections 6.2 and 6.3 are required.

(5) Lepton identification and isolation criteria
The electrons and muons need to pass the *medium* identification and *gradient* isolation criteria.

(6) Hadronic tau veto
To ensure orthogonality to the $H \to \tau_{\text{lep}}\tau_{\text{had}}$ and $H \to \tau_{\text{had}}\tau_{\text{had}}$ channels all events with one or more hadronic τ-leptons obeying the *medium* criterion are vetoed.

(7) Trigger
The event has to pass on of the triggers as defined in Section 7.2.

(8) Trigger matching
The triggered leptons have to match with the reconstructed leptons.

(9) Opposite sign
The electric charge of the two leptons has to be opposite.

(10) Dilepton mass
The mass of the dilepton systems is restricted to $30\,\text{GeV} < m_{\ell\ell} < 75\,(100)\,\text{GeV}$ for SF (DF) events. This helps to reduce the Drell-Yan $Z/\gamma^* \to \ell\ell$ background. Fig. 7.2 shows the $m_{\ell\ell}$ distribution for SF and DF events before Cut 10.

(11) Jet momentum
Jets need to have a transverse momentum of $p_{\text{T}} > 25\,\text{GeV}$. At least one jet with $p_{\text{T}} > 40\,\text{GeV}$ is required. This helps to select both the VBF and boosted category (Section 7.4). The transverse momentum distribution of the leading jet, $p_{\text{T}}^{\text{jet}_1}$, before Cut 11 is shown in Fig. 7.3.

(12) Missing transverse energy
For DF events a cut on $E_{\text{T}}^{\text{miss}} > 20\,\text{GeV}$ is applied, since neutrinos are expected in the final state. To reduce $Z/\gamma^* \to \ell\ell$ background, the requirement is tightened to $E_{\text{T}}^{\text{miss}} > 55\,\text{GeV}$ for SF events. Fig. 7.4 shows the $E_{\text{T}}^{\text{miss}}$ distribution for SF and DF events before Cut 12.

(13) Missing transverse energy (HPTO)
The missing transverse energy is calculated from only high-p_{T} objects (HPTO). Only the two decay leptons and all jets with a transverse momentum of $p_{\text{T}} > 30\,\text{GeV}$ are used.

$$\mathbf{E}_{\text{T}}^{\text{miss,HPTO}} = -\mathbf{p}_{\text{T}}^{\ell_0} - \mathbf{p}_{\text{T}}^{\ell_1} - \sum_{\substack{\text{jets} \\ p_{\text{T}} > 30\,\text{GeV}}} \mathbf{p}_{\text{T}}^{\text{jet}} \tag{7.5}$$

A HPTO missing transverse energy of $E_{\text{T}}^{\text{miss,HPTO}} > 55\,\text{GeV}$ for SF events is required to further reject $Z/\gamma^* \to \ell\ell$ background. The $E_{\text{T}}^{\text{miss,HPTO}}$ distribution is shown for SF events before Cut 13 in Fig. 7.5.

(14) Momentum fraction
The momentum fractions carried by the visible decay products of the τ-lepton decay are restricted to $0.1 < x_{1,2} < 1.0$. They are calculated in the collinear mass approximation (Section 7.1.1). This rejects background events where

the assumption of collinearity of the τ-lepton and its visible decay product is not valid. Fig. 7.6 shows the distributions of x_1 and x_2 before Cut 14.

(15) Angular difference in η

This cut limits the η difference between the two leptons to $|\Delta\eta_{\ell\ell}| < 1.5$. The $|\Delta\eta_{\ell\ell}|$ distribution before Cut 15 is shown in Fig. 7.7.

(16) Angular difference in ΔR

The ΔR separation between the two leptons is required to be $\Delta R_{\ell\ell} < 2$. Fig. 7.8 shows the $\Delta R_{\ell\ell}$ distribution before Cut 16.

(17) Collinear mass

To ensure orthogonality with the $H \to WW$ analysis, the collinear mass (Section 7.1.1) is limited to $m_{\text{coll}} > m_Z - 25\,\text{GeV}$. The m_{coll} distribution before Cut 17 is shown in Fig. 7.9.

(18) MMC mass

Events where the MMC mass reconstruction algorithm (Section 7.1.2) did not converge are discarded.

(19) b-jet veto

Events which contain b-jets (Section 6.4) with $p_{\text{T}} > 25\,\text{GeV}$ are vetoed. This helps to reduce the single-top and $t\bar{t}$ background.

Some labels of the plots need to be updated to the new indexing scheme. Also the $x_{1,2}$ distributions need a wider range.

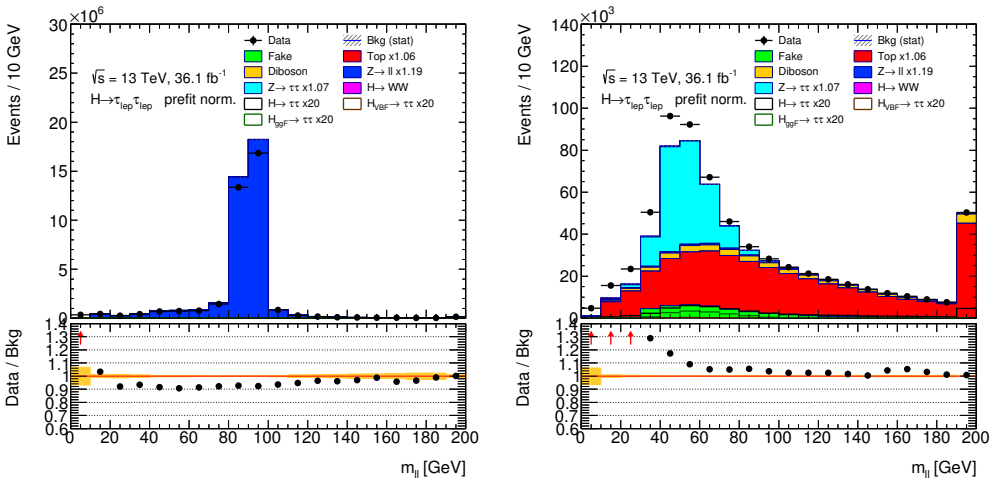

Figure 7.2: Distribution of $m_{\ell\ell}$ after Cut 9 for SF (left) and DF (right) events. Normalization factors are applied on the top-quark, $Z \to \ell\ell$, and $Z \to \tau\tau$ background. The signal is scaled by a factor of 20. Only statistical uncertainties are included in the error band.

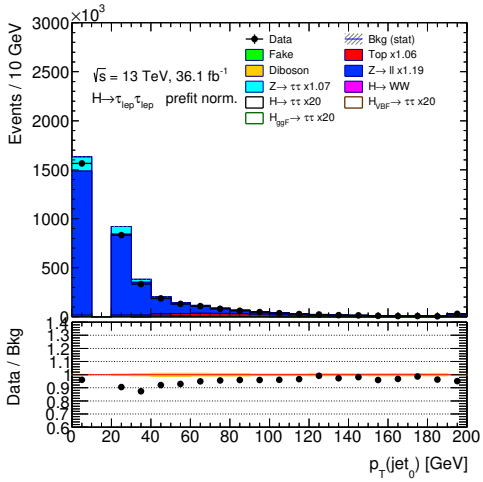

Figure 7.3: Distribution of $p_{\mathrm{T}}^{\mathrm{jet}_1}$ after Cut 10. Normalization factors are applied on the top-quark, $Z \to \ell\ell$, and $Z \to \tau\tau$ background. The signal is scaled by a factor of 20. Only statistical uncertainties are included in the error band.

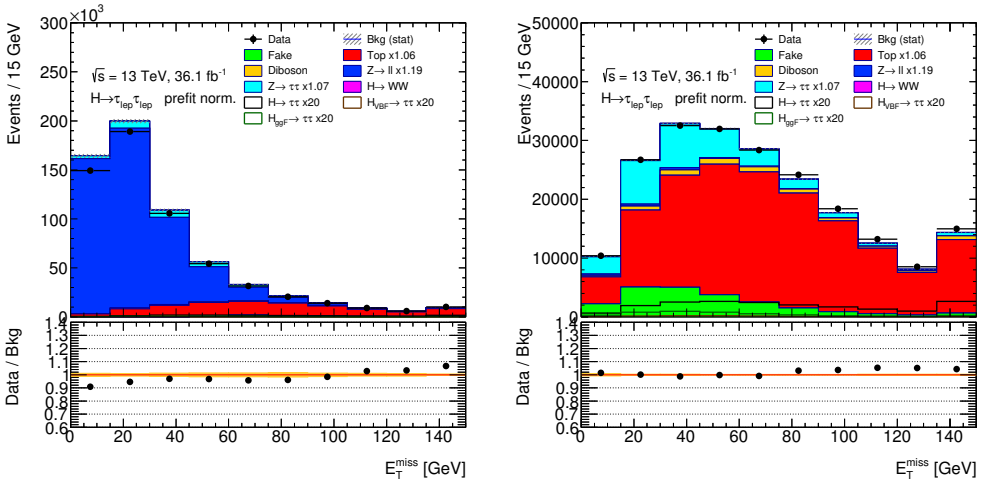

Figure 7.4: Distribution of $E_{\mathrm{T}}^{\mathrm{miss}}$ after Cut 11 for SF (left) and DF (right) events. Normalization factors are applied on the top-quark, $Z \to \ell\ell$, and $Z \to \tau\tau$ background. The signal is scaled by a factor of 20. Only statistical uncertainties are included in the error band.

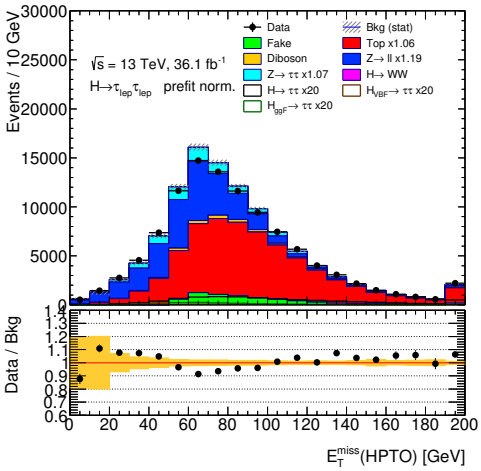

Figure 7.5: Distribution of $E_{\mathrm{T}}^{\mathrm{miss,HPTO}}$ after Cut 12. Normalization factors are applied on the top-quark, $Z \to \ell\ell$, and $Z \to \tau\tau$ background. The signal is scaled by a factor of 20. Only statistical uncertainties are included in the error band.

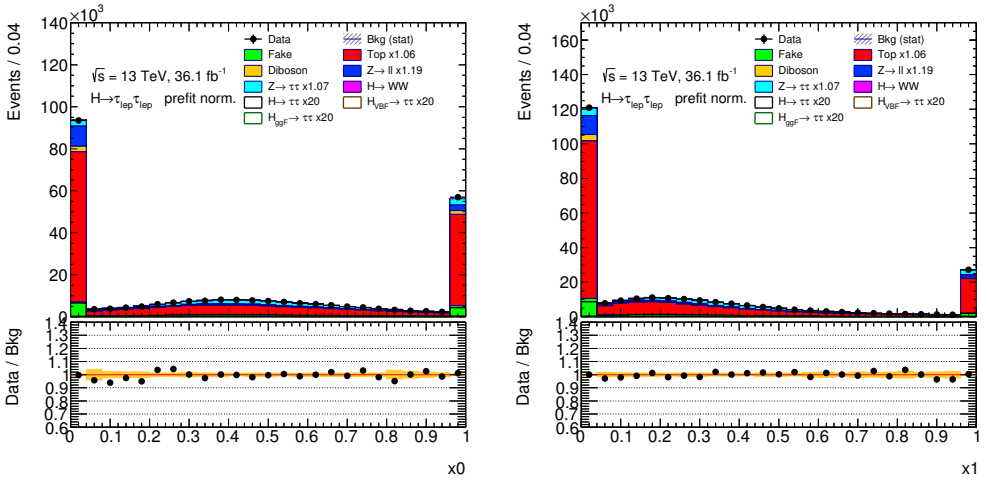

Figure 7.6: Distributions of x_1 (left) and x_2 (right) after Cut 13. Normalization factors are applied on the top-quark, $Z \to \ell\ell$, and $Z \to \tau\tau$ background. The signal is scaled by a factor of 20. Only statistical uncertainties are included in the error band.

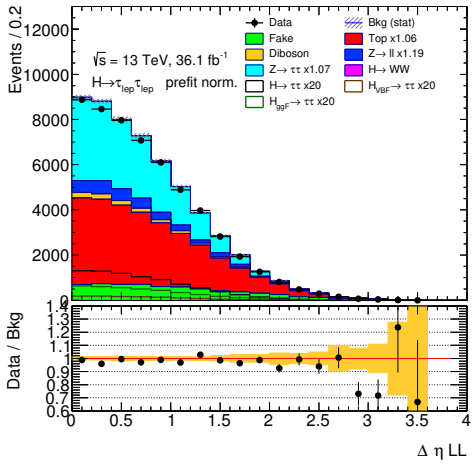

Figure 7.7: Distribution of $|\Delta\eta_{\ell\ell}|$ after Cut 14. Normalization factors are applied on the top-quark, $Z \to \ell\ell$, and $Z \to \tau\tau$ background. The signal is scaled by a factor of 20. Only statistical uncertainties are included in the error band.

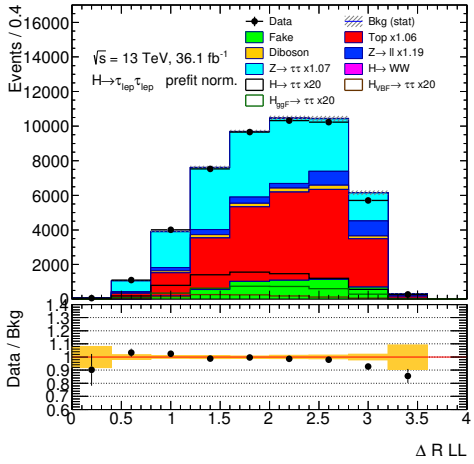

Figure 7.8: Distribution of $\Delta R_{\ell\ell}$ after Cut 15. Normalization factors are applied on the top-quark, $Z \to \ell\ell$, and $Z \to \tau\tau$ background. The signal is scaled by a factor of 20. Only statistical uncertainties are included in the error band.

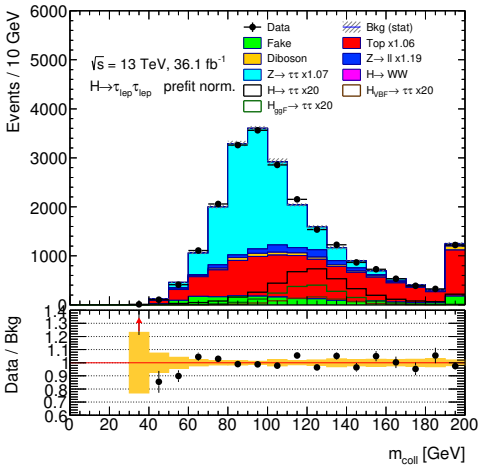

Figure 7.9: Distribution of m_{coll} after Cut 16. Normalization factors are applied on the top-quark, $Z \to \ell\ell$, and $Z \to \tau\tau$ background. The signal is scaled by a factor of 20. Only statistical uncertainties are included in the error band.

7.4 Categorization

Since the goal of this analysis is to measure the coupling strength of the Higgs boson in different production modes, dedicated categories for the VBF and gluon–gluon fusion production mode are defined by exploiting production-mode specific event topologies. They are referred to as the *VBF* and *boosted category*, respectively.

7.4.1 VBF category

In the VBF production mode two vector bosons are used to produce the Higgs boson. The vector bosons originate from two partons, which produce two jets with high transverse momentum in the forward region of the detector. The following cuts are applied to select this topology:

Add plots with variables before they are cut on.

(1V) Subleading jet momentum
A second jet is required with at least $p_{\mathrm{T}} > 30\,\mathrm{GeV}$.

(2V) Opposite hemispheres
The two leading jets need to occupy different hemispheres of the detector due to the VBF topology. This can be achieved by applying the $\eta_{\mathrm{jet}_1} \cdot \eta_{\mathrm{jet}_2} < 0$ requirement.

(3V) Angular separation of two leading jets
The separation in η between the two VBF jets is expected to be large. Therefore, a cut of $\left|\Delta\eta_{\mathrm{jj}}\right| > 3$ is applied.

(4V) Lepton candidate centrality
The η of the selected leptons must lie in between the two jets.

(5V) Invariant mass of the dijet system
The dijet system is required to have an invariant mass of $m_{\mathrm{jj}} > 400\,\mathrm{GeV}$.

Furthermore, the VBF category is split into a *high* and *low* VBF category, with requirements on the transverse momentum of the di-τ system, $p_{\mathrm{T}}^{\tau\tau} > 100\,\mathrm{GeV}$ and $p_{\mathrm{T}}^{\tau\tau} < 100\,\mathrm{GeV}$, respectively. The transverse momentum of the di-τ system is calculated from the transverse momenta of the visible decay products of the τ-leptons and the missing transverse energy. This helps to increase the sensitivity, provided that the statistics in the sub-categories are still high enough.
The distributions of m_{MMC} in the inclusive, high, and low VBF category is shown in Fig. 7.10.

Include systematic uncertainties

7.4.2 Boosted category

In contrast to the VBF production mode, the gluon–gluon fusion production mode has no outgoing partons at tree-level.However, higher order QCD corrections can produce a recoil jet, which leads to a high transverse momentum of the Higgs boson. This helps to suppress the irreducible $Z \to \tau\tau$ background. The selection criteria for the boosted category are as follows:

Ref feynman graph in theory chapter

Add plots with variables before they are cut on.

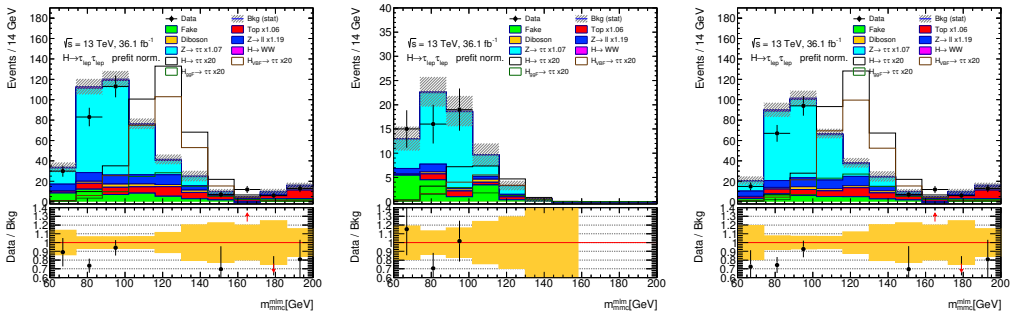

Figure 7.10: Distributions of the output of the missing mass calculator algorithm, m_{MMC}, in the inclusive (left), low (middle), and high (right) VBF category. Normalization factors are applied on the top-quark, $Z \to \ell\ell$, and $Z \to \tau\tau$ background. The signal is scaled by a factor of 20. The error band includes statistic and systematic uncertainties.

(1B) Veto on VBF selection
The events have to pass the preselection, but not the VBF selection.

(2B) Higgs boson transverse momentum
The transverse momentum of the di-τ system is required to be $p_{\mathrm{T}}^{\tau\tau} > 100\,\mathrm{GeV}$.

Similar to the VBF category, also the boosted category is divided into two subcategories. All events which pass the requirements $p_{\mathrm{T}}^{\tau\tau} > 140\,\mathrm{GeV}$ and $\Delta R_{\ell\ell} < 1.5$ are sorted into the *high-boosted* category. All other events which do not pass these criteria are filled in the *low-boosted* category.
Fig. 7.11 shows the distributions of m_{MMC} in the inclusive boosted, low-boosted, and high-boosted regions.

Include systematic uncertainties

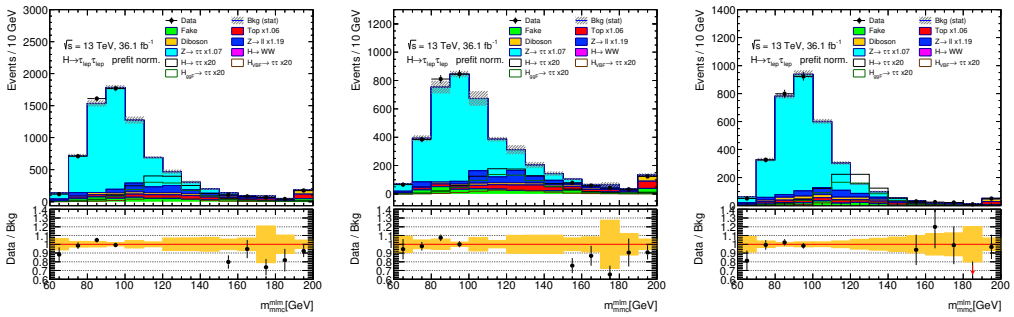

Figure 7.11: Distributions of the output of the missing mass calculator algorithm, m_{MMC}, in the inclusive boosted (left), low-boosted (middle), and high-boosted (right) boosted category. Normalization factors are applied on the top-quark, $Z \to \ell\ell$, and $Z \to \tau\tau$ background. The signal is scaled by a factor of 20. The error band includes statistic and systematic uncertainties.

7.5 Event yields

Observations in event yields

Fill out table

Table 7.3 shows the event yields for the different signal and background processes after the preselection and in the inclusive VBF and boosted categories.

Table 7.3: Event yields for the different signal and background processes after the preselection and in the inclusive VBF and boosted categories with a combined 2016 and 2016 dataset of 36.1 fb^{-1}. Normalization factors are applied on the top-quark, $Z \to \ell\ell$, and $Z \to \tau\tau$ background. Only statistical uncertainties are shown.

Process	Preselection	VBF category	Boosted category
ggF $H \to \tau\tau$			
VBF $H \to \tau\tau$			
WH $H \to \tau\tau$			
ZH $H \to \tau\tau$			
ttH $H \to \tau\tau$			
Fakes			
Top			
Diboson			
$Z/\gamma^* \to \ell\ell$			
$Z/\gamma^* \to \tau\tau$			
$H \to WW$			
Total signal			
Total background			
Data			

Bibliography

ML_HASTIE [1] T. Hastie, R. Tibshirani, and J. Friedman, *The Elements of Statistical Learning: Data mining, Inference and Prediction*. Springer, 2 ed., 2009.

ML_TMVA [2] *TMVA Users Guide*.

-SOFT-PUB-2007-007 [3] T. Cornelissen, M. Elsing, S. Fleischmann, W. Liebig, E. Moyse, and A. Salzburger, *Concepts, Design and Implementation of the ATLAS New Tracking (NEWT)*, Tech. Rep. ATL-SOFT-PUB-2007-007. ATL-COM-SOFT-2007-002, CERN, Geneva, Mar, 2007. https://cds.cern.ch/record/1020106.

-PHYS-PUB-2015-051 [4] ATLAS Collaboration, *Early Inner Detector Tracking Performance in the 2015 Data at* $\sqrt{s} = 13$ *TeV*, ATL-PHYS-PUB-2015-051, 2015, https://cds.cern.ch/record/2110140.

-PHYS-PUB-2015-006 [5] ATLAS Collaboration, *The Optimization of ATLAS Track Reconstruction in Dense Environments*, ATL-PHYS-PUB-2015-006, 2015, https://cds.cern.ch/record/2002609.

-PHYS-PUB-2015-026 [6] ATLAS Collaboration, *Vertex Reconstruction Performance of the ATLAS Detector at*$\sqrt{s} = 13$ *TeV*, ATL-PHYS-PUB-2015-026, 2015, https://cds.cern.ch/record/2037717.

LAS-CONF-2016-024 [7] ATLAS Collaboration, *Electron efficiency measurements with the ATLAS detector using the 2015 LHC proton–proton collision data*, ATLAS-CONF-2016-024, 2016, https://cds.cern.ch/record/2157687.

PERF-2015-10 [8] ATLAS Collaboration, *Muon reconstruction performance of the ATLAS detector in proton–proton collision data at* $\sqrt{s} = 13$ *TeV*, Eur. Phys. J. C **76** (2016) 292, arXiv:1603.05598 [hep-ex].

Cacciari:2008gp [9] M. Cacciari, G. P. Salam, and G. Soyez, *The anti-k_t jet clustering algorithm*, JHEP **04** (2008) 063, arXiv:0802.1189 [hep-ph].

Cacciari:2005hq [10] M. Cacciari and G. P. Salam, *Dispelling the N^3 myth for the k_t jet-finder*, Phys. Lett. B **641** (2006) 57, arXiv:hep-ph/0512210.

PERF-2016-04 [11] ATLAS Collaboration, *Jet energy scale measurements and their systematic uncertainties in proton–proton collisions at* $\sqrt{s} = 13$ *TeV with the ATLAS detector*, arXiv:1703.09665 [hep-ex].

PERF-2014-03 [12] ATLAS Collaboration, *Performance of pile-up mitigation techniques for jets in pp collisions at $\sqrt{s} = 8$ TeV using the ATLAS detector*, Eur. Phys. J. C **76** (2016) 581, arXiv:1510.03823 [hep-ex].

PHYS-PUB-2015-034 [13] ATLAS Collaboration, *Forward Jet Vertex Tagging: A new technique for the identification and rejection of forward pileup jets*, ATL-PHYS-PUB-2015-034, 2015, https://cds.cern.ch/record/2042098.

PDG [14] Particle Data Group Collaboration, C. Patrignani et al., *Review of Particle Physics*, Chin. Phys. **C40** (2016) 100001.

PERF-2012-04 [15] ATLAS Collaboration, *Performance of b-jet identification in the ATLAS experiment*, JINST **11** (2016) P04008, arXiv:1512.01094 [hep-ex].

PHYS-PUB-2016-012 [16] ATLAS Collaboration, *Optimisation of the ATLAS b-tagging performance for the 2016 LHC Run*, ATL-PHYS-PUB-2016-012, 2016, https://cds.cern.ch/record/2160731.

Run1TauPaper [17] ATLAS Collaboration, *Identification and energy calibration of hadronically decaying tau leptons with the ATLAS experiment in pp collisions at $\sqrt{s} = 8$ TeV*, Eur. Phys. J. C **75** (2015) 303, arXiv:1412.7086 [hep-ex].

PHYS-PUB-2015-045 [18] *Reconstruction, Energy Calibration, and Identification of Hadronically Decaying Tau Leptons in the ATLAS Experiment for Run-2 of the LHC*, https://cds.cern.ch/record/2064383.

LAS-CONF-2017-029 [19] ATLAS Collaboration, *Measurement of the tau lepton reconstruction and identification performance in the ATLAS experiment using pp collisions at $\sqrt{s} = 13$ TeV*, ATLAS-CONF-2017-029, 2017, https://cds.cern.ch/record/2261772.

PhysRev.185.1975 [20] J. D. Bjorken and E. A. Paschos, *Inelastic Electron-Proton and γ-Proton Scattering and the Structure of the Nucleon*, Phys. Rev. **185** (1969) 1975–1982, https://link.aps.org/doi/10.1103/PhysRev.185.1975.

PHYS-PUB-2015-023 [21] ATLAS Collaboration, *Expected performance of missing transverse momentum reconstruction for the ATLAS detector at $\sqrt{s} = 13$ TeV*, ATL-PHYS-PUB-2015-023, 2015, https://cds.cern.ch/record/2037700.

PHYS-PUB-2015-027 [22] ATLAS Collaboration, *Performance of missing transverse momentum reconstruction with the ATLAS detector in the first proton–proton collisions at $\sqrt{s} = 13$ TeV*, ATL-PHYS-PUB-2015-027, 2015, https://cds.cern.ch/record/2037904.

MCollAssumption [23] R. Ellis, I. Hinchliffe, M. Soldate, and J. V. D. Bij, *Higgs decay to $\tau^+\tau^-$ A possible signature of intermediate mass Higgs bosons at high energy hadron colliders*, Nuclear Physics B **297** (1988) 221 – 243, http://www.sciencedirect.com/science/article/pii/0550321388900193.

MColl [24] ATLAS Collaboration, G. Aad et al., *Expected Performance of the ATLAS Experiment - Detector, Trigger and Physics*, arXiv:0901.0512 [hep-ex].

MMC [25] A. Elagin, P. Murat, A. Pranko, and A. Safonov, *A New Mass Reconstruction Technique for Resonances Decaying to di-tau*, Nucl. Instrum. Meth. **A654** (2011) 481–489, arXiv:1012.4686 [hep-ex].

TauConfNote [26] A. Andreazza et al., *Measurement of the $H \to \tau^+\tau^-$ cross-section in* 13 TeV *Collisions with the ATLAS Detector*, Tech. Rep. ATL-COM-PHYS-2017-446, CERN, Geneva, Apr, 2017. https://cds.cern.ch/record/2261605.

Trigger2015 [27] ATLAS Collaboration, M. Aaboud et al., *Performance of the ATLAS Trigger System in 2015*, Eur. Phys. J. **C77** (2017) 317, arXiv:1611.09661 [hep-ex].

Trigger2016 [28] ATLAS Collaboration, *Trigger Menu in 2016*, Tech. Rep. ATL-DAQ-PUB-2017-001, CERN, Geneva, Jan, 2017. https://cds.cern.ch/record/2242069.

JetCleaning2015 [29] ATLAS Collaboration, *ATLAS TWiki*, https://twiki.cern.ch/twiki/bin/view/AtlasProtected/HowToCleanJets2015. [Online; accessed 21-September-2017].

JetCleaning2016 [30] ATLAS Collaboration, *ATLAS TWiki*, https://twiki.cern.ch/twiki/bin/view/AtlasProtected/HowToCleanJets2016. [Online; accessed 21-September-2017].